WILEY

RESEARCH ARTICLE

How much does dry-season fog matter? Quantifying fog contributions to water balance in a coastal California watershed

Michaella Chung[1] | Alexis Dufour[2] | Rebecca Pluche[2] | Sally Thompson[1]

[1]Department of Civil and Environmental Engineering, University of California, Berkeley, Davis Hall, Berkeley, CA 94720, USA

[2]San Francisco Public Utilities Commission, 525 Golden Gate Avenue, San Francisco, CA 94102, USA

Correspondence
Michaella Chung, Department of Civil and Environmental Engineering, University of California, Berkeley, Davis Hall, Berkeley, CA 94720, USA.
Email: michaellachung@berkeley.edu

Abstract

The seasonally-dry climate of Northern California imposes significant water stress on ecosystems and water resources during the dry summer months. Frequently during summer, the only water inputs occur as non-rainfall water, in the form of fog and dew. However, due to spatially heterogeneous fog interaction within a watershed, estimating fog water fluxes to understand watershed-scale hydrologic effects remains challenging. In this study, we characterized the role of coastal fog, a dominant feature of Northern Californian coastal ecosystems, in a San Francisco Peninsula watershed. To monitor fog occurrence, intensity, and spatial extent, we focused on the mechanisms through which fog can affect the water balance: throughfall following canopy interception of fog, soil moisture, streamflow, and meteorological variables. A stratified sampling design was used to capture the watershed's spatial heterogeneities in relation to fog events. We developed a novel spatial averaging scheme to upscale local observations of throughfall inputs and evapotranspiration suppression and make watershed-scale estimates of fog water fluxes. Inputs from fog water throughfall (10–30 mm/year) and fog suppression of evapotranspiration (125 mm/year) reduced dry-season water deficits by 25% at watershed scales. Evapotranspiration suppression was much more important for this reduction in water deficit than were direct inputs of fog water. The new upscaling scheme was analyzed to explore the sensitivity of its results to the methodology (data type and interpolation method) employed. This evaluation suggests that our combination of sensors and remote sensing allows an improved incorporation of spatially-averaged fog fluxes into the water balance than traditional interpolation approaches.

KEYWORDS
ecohydrology, fog, isotope analysis, water balance

1 | INTRODUCTION

Advection fog is a widespread phenomenon associated with deep marine upwelling along western continental margins worldwide (Garreaud, Barichivich, Christie, & Maldonado, 2008; Leipper, 1995). It consists of liquid-phase water with droplet sizes ranging from 1–40 μm (Prada & da Silva, 2001), small enough for droplets to be advected with wind. Fog events are thus influenced by time-varying meteorological variables such as wind speed, direction, and dew point (Azevedo & Morgan, 1974; Hiatt, Fernandez, & Potter, 2012; Weathers, Lovett, & Likens, 1995; Weathers, Lovett, Likens, & Caraco, 2000), which affect the size, density, and flux of these water droplets. Fog interaction with the terrestrial water balance occurs in three ways:

climatically, through reductions in radiation, temperature, and vapour pressure deficit, which collectively suppress evapotranspiration during fog events (Fischer, Still, & Williams, 2009); through direct water inputs, when fog droplets are intercepted by vegetation canopies and form a non-rainfall water flux that reaches the soil as canopy throughfall (Dawson, 1998; Hutley, Doley, Yates, & Boonsaner, 1997); or indirectly by alleviating water stress in plant leaves when absorbed through foliar uptake (Burgess and Dawson, 2004, Wang, Kaseke, & Seely, 2017) and reducing transpirational loss (Ewing et al., 2009; Templer et al., 2015). Fog water inputs and transpiration suppression can also enhance streamflow fluxes: isotopic tracing has unambiguously identified the signature of fog water within soil moisture, groundwater, and streamflow (Ingraham and Matthews, Ingraham

and Matthews, 1988; 1995; Scholl, Gingerich, & Tribble, 2002). Furthermore, dry-season streamflow fluctuations correlate with fog occurrence (Sawaske & Freyberg, 2015) and respond to interception mechanisms through changes in vegetation cover (Harr, 1980; 1982; Ingwersen, 1985; Keppeler, 2007). Because fog zones coincide with large arid, semi-arid, and Mediterranean climate zones, and because the fog season may also coincide with dry seasons in these regions (Fischer et al., 2009; Peace, 1969; Schemenauer & Cereceda, 1991), fog can have a significant contribution to the water balance and may increase ecosystem drought resilience (Breazeale, McGeorge, & Breazeale, 1950; Burgess and Dawson, 2004; Dawson, 1998; Haines, 1952; 1953).

Fog advects horizontally and close to the ground, and thus, terrestrial fluxes of fog water vary with topography and vegetation distribution along its advective pathway. Typically, fog inputs peak along topographic ridges and forest edges (Azevedo & Morgan, 1974; Ewing et al., 2009; Fischer et al., 2009; Vogl, 1973; Weathers et al., 1995) and vary with vegetation canopy roughness (Dawson, 1996; Shuttleworth, 1977; Wang et al., 2006). Heterogeneity in vegetation cover and a topographically complex terrain are therefore likely to generate high spatial heterogeneity in fog water fluxes. This poses a challenge in making spatially integrated estimates of fog effects on a system water balance. Most methods to estimate rates of fog throughfall rely on point-scale sampling, which has a limited ability to capture important spatial heterogeneities due to the finite density and distribution of measurement locations. Moreover, the spatial patterns adopted by fog are complex, but not random. Hence, traditional methods that assume negligible correlation between point observations beyond a certain distance (e.g., Thiessen polygon or kriging (Bacchi and Kottegoda, 1995)) are not suitable for interpolation between sampling points. Development of spatially-integrated estimation techniques that can address the complex but non-random nature of fog, as well as its interaction with a heterogeneous land surface, is needed to allow quantitative evaluation of the importance of fog water fluxes at watershed scales.

Therefore, this study seeks to answer the following questions:

1. What are the dominant controls that characterize heterogeneity of fog in a seasonally-dry, coastal watershed?
2. In what ways does fog contribute to the water balance of this system and how significant are its quantitative effects?
3. How important is each sensor and its dataset in inferring fog's watershed-scale effects?

In this study, we characterize and quantify spatiotemporal heterogeneity in fog events and deposition in a small, north coast Californian watershed during a period of extreme drought. By developing a novel spatial averaging scheme that accounts for watershed features and meteorological variables, we upscale these observations and make quantitative estimates of the hydrologic effects of fog within the watershed. We then explore the sensitivity of the upscaling scheme to changing data types, data density, and specific interpolation schemes employed while upscaling. The results highlight the importance of considering the non-random pattern of fog events when extrapolating point-scale observations to understand the hydrologic implications of fog at ecosystem levels.

2 | MATERIALS AND METHODS

2.1 | Site description

The Upper Pilarcitos Creek Watershed is a 9.6-km^2 watershed with a 630 m rise in elevation, located on the San Francisco Peninsula within the Santa Cruz Mountain range and draining into Lake Pilarcitos. It is one of the oldest components of San Francisco's water supply system and is managed within the larger Peninsula Watershed by the San Francisco Public Utilities Commission. The coastal, western divide of the watershed is covered by dense, old-growth Douglas fir forest (*Pseudotsuga menziesii*) and is characterized by highly uncompacted soil. Most of the eastern watershed is covered by chaparral rangeland; its dominant vegetation is coyote brush (*Baccharis pilularis*). The watershed averages approximately 100 cm of rain per year. It is also subject to frequent coastal fog events in summer, which, depending on wind direction, can either approach the watershed from the west, rising over a coastal ridge, or from the north or south, flowing through the river valley. During these events, the canopy of understory vegetation becomes thoroughly wet and pools of water collect beneath trees, although neighbouring grasslands remain dry (Potter, 2016); up to 150 cm of throughfall were observed over a single month under a forest canopy within a neighbouring watershed (Oberlander, 1956).

2.2 | Field methods

We deployed a suite of sensors at multiple sites in the Peninsula Watershed during three summer fog seasons coinciding with the dry season, spanning June–October in 2014, 2015, and 2016. The Peninsula Watershed is a single geologic and topographic unit in the Coast Range and experiences no geologic, vegetation, or elevation change across subwatershed boundaries created by a reservoir dam. Observation sites were located in the Upper Pilarcitos Creek Watershed and its neighbouring watersheds, which share common directional gradients in fog presence. Sites were selected to represent locations with different elevation, vegetation, wind conditions, and ocean exposure, along with variations in fog frequency, density, and approach pathways to the watershed, as reported by on-site watershed managers. Ultimately, six sites were selected covering areas of peak fog intensity (Scarper Peak and Montara Mountain, associated with a frequently occurring west-east fog pathway) and areas of less frequent fog occurrence (Spring Valley, associated with some west-east and north-south fog pathways, and Cahill Ridge, associated with a south-north fog pathway) according to operator information. Site selection, however, was constrained by accessibility limitations associated with a steep topographic slope and the presence of endangered plant and animal species, which limited sampling to locations near roads at the ridgelines and a single east-west road that spans the topographic gradient of the watershed.

Each monitoring site consisted of a throughfall collector (sloping trough: 0.3 m diameter and 1.8 m length), installed 0.6 m above ground level, and one Juvik-type radial collector (Juvik & Nullet, 1995) consisting of a 24-cm radius circular mesh, installed at 1.8–2.5 m above ground level. Each collector routed water through a sealed pipeline to its own tipping bucket rain gauge (Campbell Scientific TE525WS) recording on

5-min intervals. The two collectors were used to separately measure the vertical fog drip below the forest canopy (throughfall collector) and the horizontal component of wind-driven fog, or the amount of water transported horizontally by fog through the canopy system (radial collector). We interpret the radial collector data to provide an index of the advection fog flux density (volume water per area per time), allowing comparisons to be made between similar fog events in different locations. The fog collection sites spanned elevations from 245 to 580 m on both the west- and east-facing hillslopes (Figure 1 and Table 1) and covered the two dominant vegetation types of the watershed: Douglas fir forest and coyote brush scrub. The east-facing forest sites were located under varying forest conditions, with Montara Mountain at the forest edge and both Scarper Peak sites further in the forest stand.

Additionally, a weather station was deployed on each hillslope of the watershed. The weather stations (HOBO H21-002 Micro Station) logged local air temperature and relative humidity. A third weather station, a Remote Automatic Weather Station (RAWS), was already present at Spring Valley Ridge and recorded hourly precipitation, wind, solar radiation, temperature, and relative humidity. At three sites, soil moisture sensors (Decagon 5TM time domain reflectometers) were installed 75 mm and 300 mm below the surface to measure the soil

volumetric water content (VWC) and temperature responses to fog drip; these sensors measure VWC using capacitance/frequency domain technology to determine the dielectric constant of soil and measure temperature using a built-in thermistor. Additionally, five leaf wetness sensors (Decagon LWS) were deployed, four along a topographic gradient on the east-facing hillslope and the fifth sensor co-located with a fog collection site in the forest stand. The leaf wetness sensors measure the accumulation of water on a surface with equivalent thermal properties to a leaf. All leaf wetness sensors were placed horizontally, 1–2 m off the ground in the under-storey of even-aged Douglas fir stands, minimizing the effect of vegetation change on observed wetness. During a fog event, accumulation of water is presumed to derive from fog impaction. This deployment is widely used to sample fog occurrence and strength, as it provides a relatively stable range of response to leaf surface wetness and minimizes water running off the sensor surface for small collected water volumes (Cobos 2013). Lastly, two time-lapse cameras (Brinno TLC200), recording images at 30-min intervals with viewsheds facing west and southward and aligned with major fog flow pathways, were installed on Spring Valley Ridge. All data were complemented by notes from weekly field visits, during which visual observations of fog presence and location were recorded.
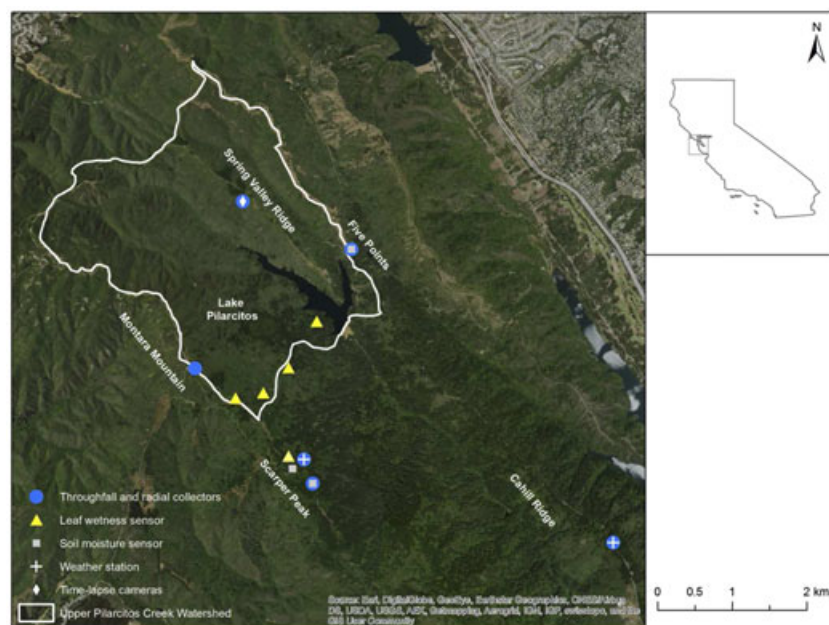

FIGURE 1 Map of Upper Pilarcitos Creek Watershed: study sites and instrumentation location

TABLE 1 Descriptions of each study site

Site	Elevation (m)	Dominant vegetation	Distance from forest canopy edge (m)	Aspect
Five Points	258	DF	91	W
Cahill Ridge	321	DF	122	W
Spring Valley Ridge	329	CB		W
Scarper Peak 1	554	DF	135	E
Scarper Peak 2	581	DF	197	E
Montara Mountain	548	DF	20	E

Note. DF is Douglas fir and CB is coyote brush canopy; W is west-facing and E is east-facing hillslope.

Stream water, non-green, non-photosynthetic stem and tissue (e. g., tree twigs), and soil samples were collected throughout the fog season in 2014 and 2015 for stable isotope analysis. Fog samples were collected at three sites using harp-style passive collectors (Fischer & Still, 2007) over a 24-hr period: The collectors were set up during a field visit with foggy conditions, and the samples were retrieved the next day to avoid evaporative effects. Water samples were extracted from stem and soil samples by cryogenic vacuum distillation and stable hydrogen and oxygen isotope compositions were determined at the Center for Stable Isotope Biogeochemistry at Department of Integrative Biology, University of California, Berkeley. The ratio of concentration of deuterium to ^{1}H, δD, in water was analyzed in dual inlet (DI) using a hot chromium reactor unit (H/Device) interfaced with a Thermo Delta Plus XL mass spectrometer. Multiple standards were added to every run, and different isotope ratios were used to correct for differential drift in standards. Long-term external precision is ±0.80. The ratio of concentration of ^{18}O to ^{16}O, δ^{18}O, in water was analyzed by continuous flow (CF) using a Thermo Gas Bench II interfaced to a Thermo Delta Plus XL mass spectrometer. A volume of water (20–200 μl, depending on the sample volume available) for both standards and samples was pipetted into 10 ml glass vials and quickly sealed. The vials were then purged with 0.2% CO_2 in helium and allowed to equilibrate at room temperature for at least 48 hr. The δ^{18}O in the CO_2 was then analyzed. Long-term external precision is better than ±0.12. For QA/QC, two lab standards were analyzed between every 20 samples.

2.3 | Soil moisture analysis

Soil moisture-fog analysis was conducted using Pearson's correlation coefficient to estimate the linear correlation between soil VWC and fog throughfall data from one site (Scarper Peak 1). To evaluate changes in this correlation between different times of the fog season, we compared the correlation coefficient of the entire fog season (June–October) to the coefficient from early summer (June, July) and late summer (August, September).

2.4 | Evapotranspiration estimates

We estimated potential open water evaporation from Lake Pilarcitos and potential evapotranspiration (PET) for forest and chaparral canopies, using the Priestley-Taylor equation (Priestley & Taylor, 1972) and RAWS data and local data from deployed weather stations. Differences in open water evaporation and PET on foggy and clear days were used to estimate PET reduction due to fog for chaparral and forest canopy at a daily timescale. PET reduction estimates for each canopy were multiplied by the average number of foggy days per dry season to find a vegetation area-weighted estimate of avoided evapotranspiration loss for the watershed.

Reduction in solar radiation during a fog event was calculated by finding the average percentage reduction in daily solar radiation between clear and foggy days, classified based on fog collector data.

2.5 | Upscaling scheme

The upscaling approach involved 8 steps, which are shown conceptually in Figure 2.

We assumed that the primary control on fog throughfall was the presence/absence of fog at any x-, y-coordinate location in the watershed. Based on discussions with watershed managers, visual field observations, time-lapse camera data, and analysis of Landsat records over a 20-year period (1991–2011), we developed four classifications
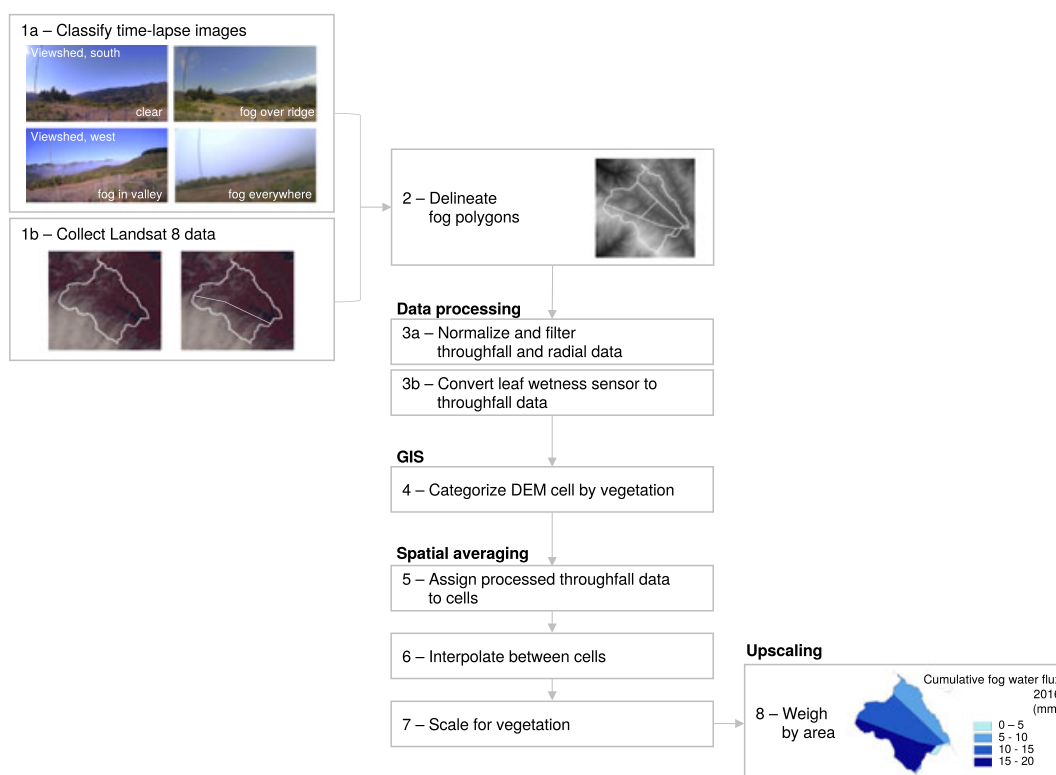

FIGURE 2 Schematic diagram of spatial averaging scheme. DEM = digital elevation model

of fog extent, which were used to constrain the locations in the watershed over which fog occurred during any given event. We then assumed that the secondary control on throughfall occurrence was the elevation of the fog ceiling and thus the interaction of fog with local vegetation canopy. This fog ceiling elevation was assumed to be homogeneous throughout the area in which fog occurred. The effect of watershed elevation on wetness, as a proxy for fog-canopy interaction, was accounted for using a transect of leaf wetness sensors that spanned the elevation range of the watershed. We note that other effects of elevation, for example, on temperature and moisture in the atmosphere, are generally negligible over the elevation range in the Upper Pilarcitos Creek Watershed under conditions of the Californian coastal climate (Mooney & Zavaleta, 2016). Furthermore, because different vegetation canopies exhibit varying roughnesses and vertical extents, we expected different quantities of throughfall under different canopies given fog presence at a given elevation. These tertiary canopy-related effects were controlled for by comparing throughfall for equivalent densities of advection fog between different vegetation types.

Therefore, the upscaling scheme firstly subdivides the watershed into places where fog occurs or does not, then controls for variations in the cloud ceiling within the fog-bound areas, and then adjusts these factors using vegetation to make an estimate of throughfall. This approach implicitly assumes that the elevation of the fog ceiling is comparable across the area where fog occurs and independent of vegetation type, and that there are no additional interactions between throughfall, watershed elevation, and vegetation—an assumption supported by the well-mixed atmospheric conditions that typically prevail in the California coastal area.

We note that our upscaling scheme focuses on the Upper Pilarcitos Creek Watershed, located at the upper half of the Peninsula Watershed, as water balance computations can occur at the dam, but this boundary is not physical and has no influence on fog dynamics.

Step 1. For each day during the fog season, we manually classified time-lapse images from 7 a.m. to 3 p.m. according to fog presence and location within each camera's viewshed. This time window was chosen as images from outside this window were too dark for classification. The first camera's viewshed included Montara Mountain and its east-facing hillslope, whereas the second camera's viewshed included Scarper Peak and its east-facing hillslope. Four classifications were used for each viewshed: clear, fog over ridge, fog in valley, and fog everywhere. All images could be unambiguously classified into one of these groups. The "clear" classification was used when there was no interaction of fog or low-lying clouds with the vegetation canopy in the image. The "fog over ridge" classification was used when fog was interacting only with the canopy along the ridgeline and the "fog in valley" classification was used when fog was observed only at low elevations on the hillside. The "fog everywhere" classification was used when the entire image was blurred by fog.

Next, the classified images were compared to images from Landsat 8. We collected remote sensing images from the same time period showing fog over the watershed.

By relating the broad spatial patterns seen in the Landsat images to each of the four classifications from the time-lapse images, we were able to delineate general coverage extents of each classification. Although only 5 fog images could be identified that overlapped with the study period, Landsat 5 images from fog seasons over a 20-year period, as well as watershed site visits, confirmed the four patterns. These boundaries, which most importantly show the edge line of the typical fog event in the watershed, were drawn in ArcGIS to create Landsat polygons.

Step 2. A set of Thiessen polygons was created in ArcGIS using the larger Peninsula Watershed boundary and all throughfall collector locations. These polygons were then trimmed to the Upper Pilarcitos Creek Watershed, noting the importance of boundaries in precipitation interpolation (Dale and Fortin, 2014). The boundaries of the Thiessen polygons were combined with those of the Landsat polygons from Step 1 by overlapping the two sets of polygons' boundaries. These new polygons consider the distance-based spatial correlations that form the basis of conventional interpolation methods while retaining the spatial extents of the fog events that occur in the watershed. The polygons act as the general framework for our spatial averaging scheme.

Step 3. The throughfall and radial collector data were normalized and filtered for any rainfall using precipitation data from the RAWS to isolate the effects of fog on the water budget. Because fog can register on a rain gauge but at much smaller volumes than rainfall, we compared two rain gauges, one located at the RAWS, where fog occurs, and the other located at Lake Pilarcitos, where fog is rare due to low elevation, to find a threshold rain gauge reading for rainfall water inputs. Precipitation was assumed to be rain-derived if RAWS-recorded data exceeded 0.25 mm per precipitation event, and throughfall and radial collector data from those time periods were set to zero so that we would not include rainfall water measurements in our fog water estimates.

Step 4. Using a vegetation map superimposed on a 3-m digital elevation model (DEM) of the Upper Pilarcitos Creek Watershed in ArcGIS, we categorized each elevation cell (3 × 3 m pixel) according to land and vegetation type (e.g., water, chaparral, and forest). The DEM was then disaggregated into smaller DEMs corresponding to the polygons from Step 2.

Step 5. For each 5-min time step, we assigned a subset of gauge points for each polygon. Each gauge point describes a location used in interpolation (Step 6) within each polygon. In polygons containing a fog measurement site, the site (with its throughfall data and elevation) served as the main gauge point, and secondary gauge points were the leaf wetness sensors. In polygons that did not enclose a fog measurement site, such as those covering the area between Montara Mountain and Spring Valley Ridge, data from another fog measurement site was assigned to the main gauge point, based on the time-lapse image classification and thus presence and location of fog at the time step. For example, in a polygon between Montara Mountain and

Spring Valley Ridge, the main gauge point was set to zero for a "fog over ridge" classification because the time-lapse image showed fog only over the Montara Mountain ridge; for a "fog in valley" classification at another time step, for which the time-lapse image showed fog only in the lower elevations, the main gauge point was assigned throughfall data from Spring Valley Ridge, an adjacent lower elevation site. For a "clear" classification, when no fog was observed in any polygons by the time-lapse image, the main gauge point was set to zero.

Step 6. Within each polygon, the elevation cells that matched the elevations for the main and secondary gauge points were assigned corresponding data. Assuming a linear increase of moisture with elevation, we interpolated throughfall values for the remaining elevation cells. This assumption was based on regression analysis of throughfall data, which showed a linear effect of elevation on throughfall. Two sets of data from three fog seasons were considered: (a) daily throughfall data given fog presence from fog collectors from all forested sites except for Montara Mountain, spanning a range of elevation with similar forest stand conditions and (b) potential throughfall from leaf wetness sensor data from the four sites along a topographic gradient. Leaf wetness counts were converted to corresponding throughfall values to estimate potential throughfall from leaf wetness sensors: previous work (Koohafkan, Thompson, & Dawson, 2014, unpublished material) using a simulated fog chamber showed that leaf wetness sensors respond near-linearly to wetness inputs below a sensor reading of 820 counts, and therefore, given a wetness count value for dry conditions, it is possible to predict fog water inputs from wetness counts. Though our range of leaf wetness counts exceeded 820, with the maximum around 1,000 counts, we found that the difference between the linear relationship between throughfall and leaf wetness counts for the range of sensor readings below 820 counts and the entire range observed was negligible. For each fog season, in which leaf water accumulation and throughfall total time series are stationary, we performed a regression to find a linear model that best predicts co-located throughfall volumes from leaf wetness counts ($R^2 = 0.38$–0.52). This linear model conversion provides supplementary estimates of potential throughfall at a higher spatial resolution along an elevation gradient.

Linear regressions on each set of data showed consistent and significant elevation scaling for throughfall (slope, $m = 0.0048$ [data set 1], 0.0049 [data set 2]) despite noisiness of data ($R^2 = 0.06$ [data set 1], 0.15 [data set 2]). Therefore, fog collector throughfall data for the main gauge point and potential throughfall from leaf wetness sensors for the secondary gauge points were used to scale for elevation in the remaining elevation cells.

Step 7. To account for vegetation effects on throughfall (Section 3.1) and avoid over-estimation of throughfall in chaparral, we scaled down throughfall measurements in the chaparral elevation cells in polygons where the gauge points were under forest canopy. In polygons where the gauge points were under chaparal canopy, throughfall measurements in the forest elevation cells were scaled up. Water cells, with no vegetation, were set to zero.

Step 8. We found a polygon-scale throughfall estimate for each polygon by estimating an area-weighted average of each elevation cell's throughfall measurement. We then calculated a watershed-averaged throughfall by estimating an area-weighted average of the polygon-scale throughfall estimates.

Following this scheme, we developed a time series for watershed-averaged fog water flux for 2014, 2015, and 2016.

To evaluate the effect of the data sources and interpolation methods on our upscaling scheme, we compared the watershed-averaged estimates of fog water flux calculated from 10 different schemes with varying data types. Our presented scheme uses data from all throughfall collectors and leaf wetness sensors, as well as time-lapse classifications, Landsat 8 imagery, the watershed vegetation map, and DEM (Table 2, Scheme 4). The nine other schemes were created using a factorial combination of the data sources, presented in Table 2. To evaluate the effect of data density, we systematically limited the number of throughfall collectors and leaf wetness sensors contributing to the final scheme.

TABLE 2 Sensors and datasets included in each upscaling scheme

	Throughfall	Leaf wetness sensor	Landsat	Vegetation	DEM
1	×				
2	×	×			
3	×	×	×		×
4	×	×	×	×	×
5	×	×		×	×
6	×	×			×
7	×		×		
8	×		×	×	
9	×			×	
10	×	×		×	

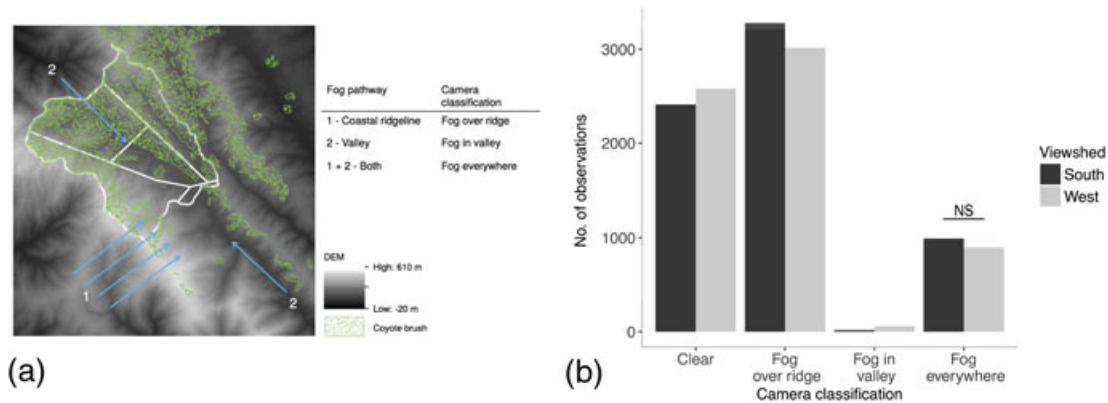*Note.* DEM = digital elevation model.

FIGURE 3 Two fog pathways were identified in the watershed; the coastline ridge pathway was most frequent, resulting in fog's accumulation on the western ridge. The watershed and its neighbouring watersheds share similar fog pathways, vegetation (dominant types and cover), and topographic gradients. In an analysis of camera viewsheds and fog classifications, all viewsheds and classifications were found to be statistically different except where noted in the figure

3 | RESULTS

3.1 | Observed heterogeneities in fog events and deposition

There were 89 foggy days in 2014, 74 in 2015, and 63 in 2016, occurring on 73%, 61%, and 52%, respectively, of days during each dry season. Two approach pathways of fog to the Upper Pilarcitos Creek Watershed were identified, shown in Figure 3(a): The most frequently occurring, around 83% of all foggy days, was over Montara Mountain from the coast, which caused the fog to accumulate on the western ridge of the watershed. The other, less frequent but concurrent when present with the first pathway, occurred in valleys, through which the fog travels (a) toward Lake Pilarcitos from its west fork branch and (b) to Cahill Ridge from the south; the valley pathways occurred around 17% of foggy days (Figure 3(b)).

The high-elevation, forest canopy sites on the east-facing hillslope received the highest amount of moisture from fog, with a decline moving down-slope and inland within the vegetation canopy. The forest edge site with direct wind and ocean exposure recorded up to three times the volume of seasonal cumulative throughfall compared to the sites located at similar elevation but situated >50 m within the forest stand (Figure 4, Montara Montain vs. Scarper Peak; illustrative data for 2016). The leaf wetness sensors also showed wetter conditions at the forest edge than interior (Figure 5(a); illustrative data for 2016). However, frequency of wetness events (period of consecutive record) between forest edge and interior sites varied between years. In some years, the percentage of the season during which leaf wetness sensors recorded wet conditions was similar at both sites, whereas in others, higher frequency of wetness events at the forest edge was observed. Leaf wetness counts generally declined with decreasing elevation along the east-facing hillslope (Figure 5(b); illustrative data for 2016). The 400- to 500-m elevation band of the watershed experienced the wettest conditions for the highest portion of the dry season, with highest average leaf wetness counts observed around 470 m but also with higher variability at this elevation, whereas below 300 m, there was a sharp decrease in wet conditions.

We also observed differences in fog-derived moisture with vegetation type. For equivalent advection-fog intensities as measured in the
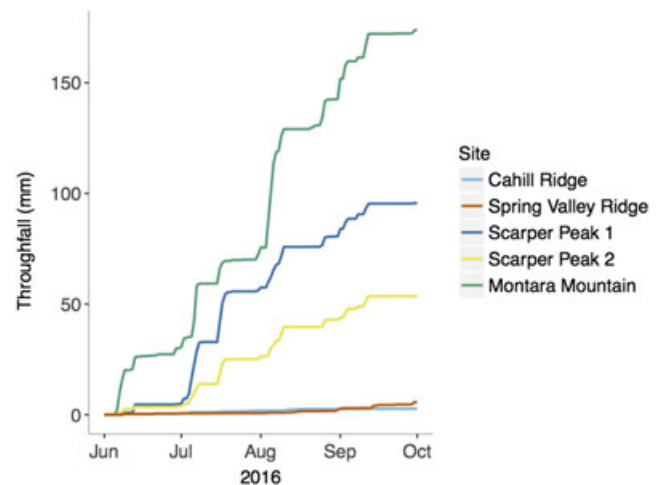

FIGURE 4 Cumulative throughfall at each fog study site in 2016: The high-elevation forest canopy sites (Scarper Peak, Montara Mountain) on the western water divide, with direct ocean and wind exposure, received the highest amount of moisture from fog. Results from all 3 years are discussed in the text

radial collectors, less fog was captured under chaparral than forest canopy (Figure 6; illustrative data for 2016), although these differences varied in their magnitude: 5:1 vs. 6:1 vs. 28:1 in 2014 vs. 2015 vs. 2016. It is also important to note that because the radial collector measured advection fog at only one elevation per site, its data are unable to distinguish between the absence or reduced bulk intensity of fog and a lifting of the fog ceiling. In 2014 and 2016, advection fog occurred with higher frequency and intensity along the open, wind-exposed chaparral ridgeline of Spring Valley Ridge than on forested Scarper Peak; in 2015, advection fog intensity was similar at the two sites. For the same intensity of advection fog, lower throughfall measurements were observed at the chaparral site than at the forest sites. Furthermore, although the increase in fog advected through the canopy signifies greater availability of moisture for interception by vegetation, less throughfall occurred overall at the chaparral site than at the forest sites.

Lastly, the three study years showed considerable temporal variability in fog intensity and event size (Figure 7). Between 2014 and 2015, the size of the average fog event and fog event frequency
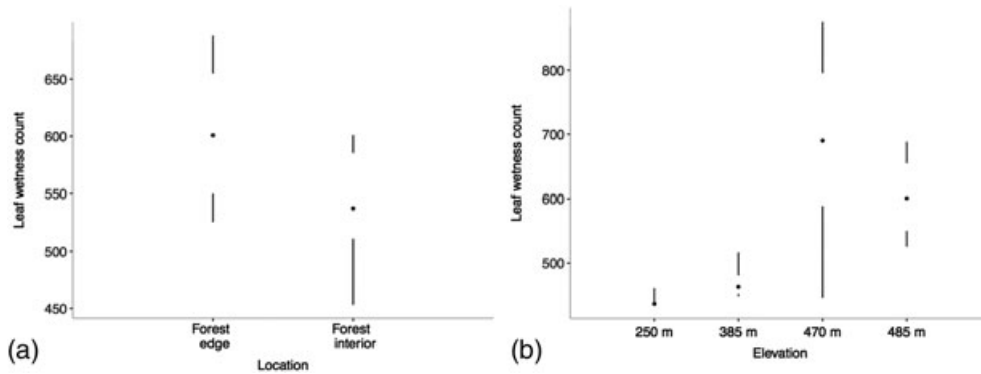
FIGURE 5 Daily average leaf wetness counts during a representative foggy period (2016) by (a) site forest conditions and (b) site elevation. Wetness counts generally decrease with elevation down a hillslope and are reduced with distance into the forest stand during this illustrative period in 2016. Results from all 3 years are discussed in the text. The point indicates the median and the gap indicates the interquartile range. One site is presented for each category
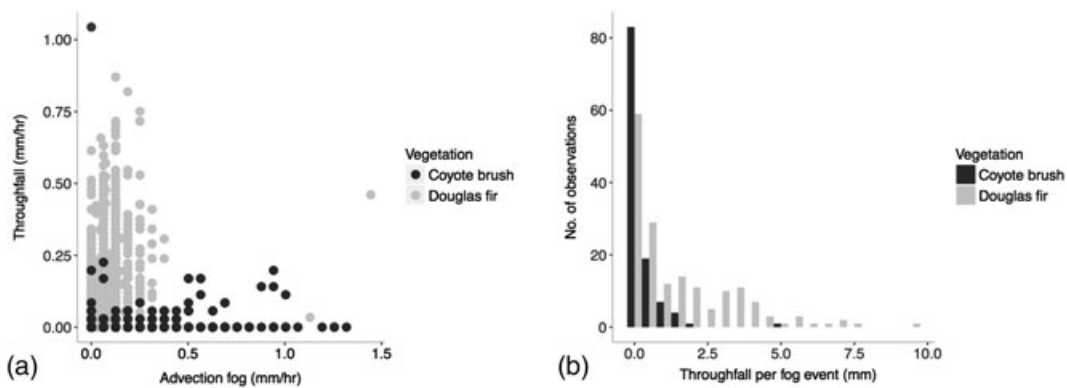

FIGURE 6 The difference in throughfall observations under chaparral and forest canopy are shown through (a) the relationship between advection fog and throughfall in 2016 (b) a histogram of fog event size from 2014–2016
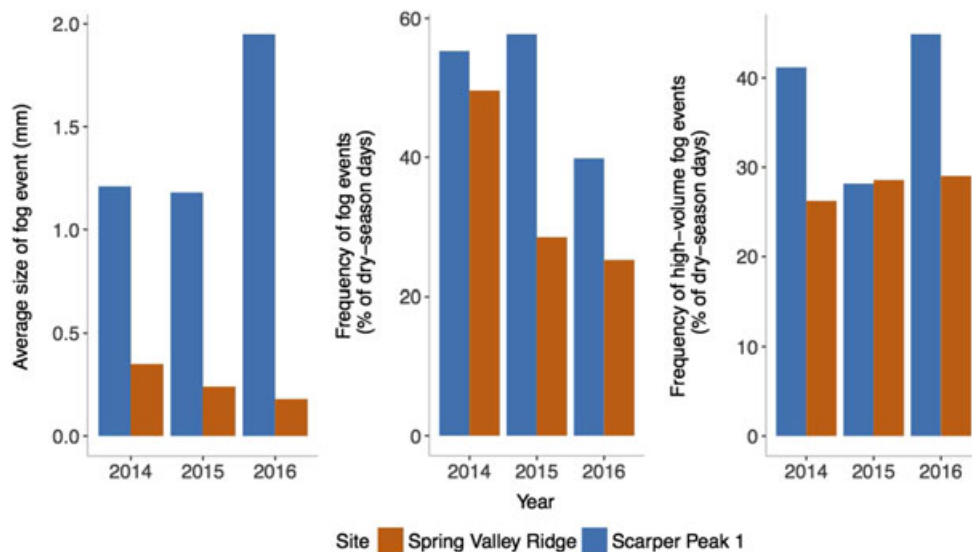

FIGURE 7 Comparison of average size and frequency of fog events shows interannual variability. High-volume fog events are events recording volumes higher than the seasonal average

decreased markedly at Spring Valley Ridge, with a 62% decrease (21.5 vs. 8.2 mm/season) in throughfall. This was related to a 96% decrease (12.4 vs. 0.5 mm/season) in horizontal transport of fog measured by the radial collectors. At Scarper Peak, the size of the average fog event

and fog event frequency remained the same between 2014 and 2015, though the frequency of high-volume fog events, or events recording volumes higher than the seasonal average, was reduced. Between 2015 and 2016, the size and frequency of fog events decreased further at
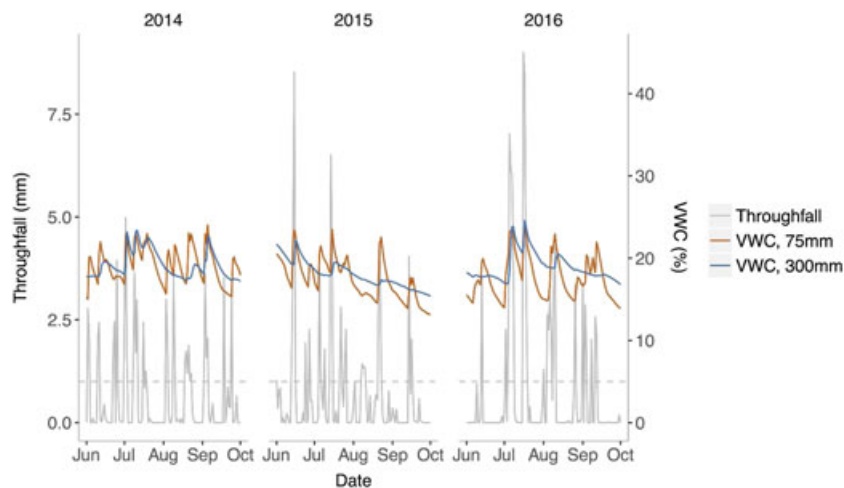
FIGURE 8 Normalized throughfall and volumetric water content of subsurface soil: Changes in soil moisture occur when fog events produce daily throughfall volumes greater than 1 mm, as indicated by the horizontal dashed line. VWC = volumetric water content

Spring Valley Ridge (8.2 mm/season vs. 5.7 mm/season), though horizontal transport of fog increased at all sites to volumes exceeding those in 2014. At Scarper Peak, the size of the average fog event increased, whereas fog event frequency decreased by a third from the previous year, resulting in similar throughfall volumes observed through the three years at this site.

3.2 | Watershed-scale effects of fog on water balance

Using the upscaling scheme, we estimated a watershed-averaged monthly input of fog water flux of 6.7 mm contributing directly to the Upper Pilarcitos Creek Watershed during the 2014 fog season, an average of 2.6 mm in 2015 and 2.9 mm in 2016 ($\sigma^2 = 0.02$ mm). This results in 10–30 mm/year of additional water flux from fog, or 1–3% of the total water input to the watershed. The decrease in direct water input in 2015 and 2016 is largely due to the decrease in throughfall in interior, low-elevation chaparral sites, as recorded at Spring Valley Ridge, which represents much of the watershed area.

Soil moisture peaks under forest canopy were weakly positively correlated with fog events and correlation decreased with depth from the soil surface over the entire fog season ($r = 0.36$, $r = 0.15$ at 75 mm and 300 mm below surface). Such correlation coefficients are dependent on timing during the dry season, however, with values decreasing from the early months of the season (June, July) to the late months (August, September): r decreases from 0.46 to 0.21 at 75 mm and from 0.15 to no correlation at 300 mm below surface. The average volumetric water content of soil was greater following periods of persistent fog (three or more consecutive days of fog events) than during clear, no-fog periods, at both depths in the soil column ($p < .05$, one-sided t test), but soil moisture responded only to throughfall percolating into the soil during above-average events (>1 mm/day; Figure 8).

The isotopic composition of fog, stream, soil, and stem water samples are presented in Figure 9. Fog water was enriched with heavy isotopes of deuterium and ^{18}O compared to rain. Though the isotopic signature of fog samples plot along the local meteoric water line, fog could not have been generated from local water sources given the proximity to the coast and the prevailing summer conditions. By contrast, stream water samples showed a similar isotopic signature to rain
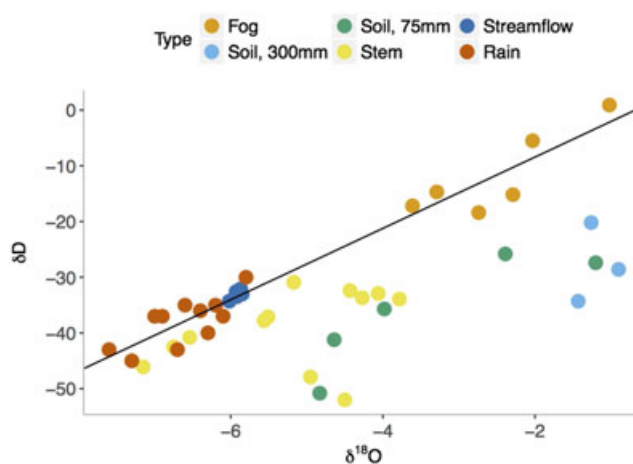

FIGURE 9 Water isotopes of rain (Ingraham & Matthews, 1995), fog, stream, soil, and vegetation stem. LMWL represents the local meteoric water line (based on fog and rain data, $\delta D = 4.4 + 6.4\delta^{18}O$)

(i.e., depleted in composition) and exhibited little variation over time. Stem water, representing water sourced by vegetation, and shallow soil water samples exhibited similar isotopic composition to streamwater. The temporal variation in signature of soil water, however, did not correspond to trends in fog events (e.g., occurrence or duration), reflecting the low correlation between fog events and changes in soil moisture observed in the watershed.

During the fog season, the total PET was 570 mm. Changes in climatic variables resulted in a 9.5% decrease in potential open water evaporation from Lake Pilarcitos between clear and foggy days (3.3 vs. 3.0 mm/day). At a high-elevation, forested site with direct ocean exposure, there was a 37% reduction in PET on foggy days and, at the open, chaparral site, a 17% reduction. We note that the radiometer was located at the chaparral site, which often experienced clear conditions while the forested site was under fog. When fog events occurred, there was a 7% average reduction in solar radiation; considering this decrease on foggy days, we found a 41% reduction in PET at the forested site. Considering these magnitudes of PET reduction, there was an approximate decrease in transpiration demand of 125 mm/year from fog.
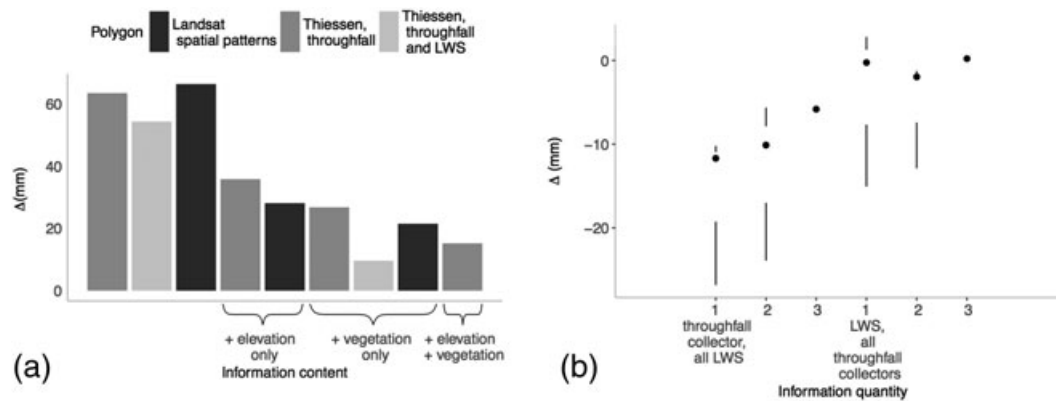
FIGURE 10 Considering the highest information content scheme as our baseline, decreasing the (a) number of data types and (b) data density results in an increase in deviation from the baseline. LWS = leaf wetness sensor

3.3 | Sensitivity of upscaled values to data sources and interpolation methods

Relative to the final scheme with the highest information content, which we considered as our baseline estimate of watershed-scale fog water flux, the loss of data types in the nine other schemes resulted in increasing deviation from the baseline estimate. The deviation from the baseline when supplementary watershed data was not included is shown as the difference in the three-season totals between each scheme and the final scheme, Δ, which increased when either vegetation or elevation data were not considered (Figure 10(a)). We found that the upscaled estimates were sensitive to an omission of vegetation cover data, whereas the omission of elevation data had a lower impact. The same trends were observed when comparing the average difference of upscaled totals at the original 5-min time step. Once these data were added, the watershed-scale estimate remained sensitive to the inclusion of Landsat data: The use of Landsat-based polygons, which combine Landsat-observed patterns with Thiessen polygons per our upscaling scheme, generally resulted in a reduction in Δ. On the other hand, the use of Thiessen polygons created from throughfall collector locations resulted in increased Δ. Furthermore, Δ was reduced through an increase in number of throughfall collectors at forested sites on the east-facing hillslope, but fog water flux estimates were less sensitive to an increase in the number of leaf wetness sensors along a topographic gradient (Figure 10(b)).

4 | DISCUSSION

The dominant controls of heterogeneity in fog occurrence and flux in the Upper Pilarcitos Creek watershed are both spatial and temporal: topography, vegetation, and interannual variability. High-elevation sites with direct wind and ocean exposure experienced the highest frequency of fog events, and this high volume of fog throughfall decreased with lower elevation. As fog advects inland through the watershed and elevation decreases, the vegetation canopy begins to lower, and its interaction with the fog ceiling is reduced. The fog also begins to evaporate as it moves inland, reducing the advective fluxes of fog water, and thus fog-vegetation interception. Our observations of substantial fog water flux at the high-elevation, ridgeline sites, and negligible flux at low elevations east of the ridge reflect findings of

previous studies (Fischer et al., 2009; Sawaske & Freyberg, 2015). We, however, find a reduced difference in magnitude of flux totals between these two elevations and forest conditions: a comparison of daily leaf wetness counts from a ridge site and a lower hillside site shows that the ridgeline had counts that were on average 1.1 times higher (with a 2-times maximum), compared to a 70-fold increase in monthly throughfall rates found by Sawaske and Freyberg (2015) in the same region. Vegetation cover and type also serve as major determinants of spatial heterogeneity. The leaf wetness sensors showed wetter conditions at the forest edge than interior, from which we infer that interaction with the vegetation canopy decreases the droplet density and advective flux. We also found that throughfall totals averaged 4-fold higher in the edge than compared to the interior of the forest, similar to a 6.6-fold increase seen by Ewing et al. (2009). Furthermore, physical differences in vegetation type across the watershed affect canopy interception of fog and subsequent fog water flux. Forest and chaparral canopies differ in height: Whereas coyote brush scrub are generally smaller than 1.5 m, Douglas fir trees reach to 70 m, increasing frequency of fog-canopy interaction. The needle-like leaf surface of Douglas fir shoots also provides more surface area than the small, round leaves of coyote brush for fog to impact and on which droplets can accumulate.

In addition to their spatially heterogeneous nature, the frequency and intensity of fog events varied between fog seasons. For example, the intensity of advection fog fluctuated over the study years, decreasing between 2014 and 2015, and increasing in 2016. This can potentially be attributed to changes in sea surface temperature (SST) anomalies in the north Pacific Ocean basin (Johnstone & Dawson, 2010). The 2014 fog season saw above-average SSTs in the eastern basin starting and peaking in mid-July (+3 °C). In 2015, however, such anomalies began earlier in June and remained +3–3.5 °C until the end of August (NOAA Office of Satellite and Product Operations, 2015). Because above-average SST anomalies decrease the ocean-land pressure gradient that drives the coast-to-inland advection of fog, an increase in anomalies in 2015, especially during the month of August when historically, fog events reach maximum frequency, may have resulted in decreased intensity of fog events for the season. SST anomalies were minimal in the summer of 2016 (NOAA Office of Satellite and Product Operations, 2015), potentially facilitating the advection of fog into the watershed.

The new upscaling scheme allows us to incorporate these spatiotemporal controls on point-scale observations to further our understanding of how fog events affect the watershed hydrologic cycle. The Upper Pilarcitos Creek Watershed receives 1,000 mm/year of rainfall. In this basin, the direct water additions from fog, 10-30 mm/year, are relatively minor but comparable to other studies (Ewing et al., 2009; Sawaske & Freyberg, 2015). The addition of a water flux from canopy interception of fog results in wetting of the shallow subsurface, with greater average volumetric water content of soil from the surface to 300 mm below following periods of persistent fog. Low correlation between soil moisture upticks and throughfall, however, is likely due to soil moisture's response to throughfall from above-average fog events early in the dry season. After August, the deeper soil likely experiences a dry-down, in which soil below the sensor becomes dried out such that the soil is unaffected by additional moisture. As this soil stops responding to throughfall pulses, even lower correlation coefficients between soil moisture upticks and throughfall are observed. Although fog water was enriched with heavier isotopes than rain, as fog represents early-stage condensate that is not subject to the "rain-out" effect, or depletion throughout a precipitation event (Dawson, 1998), similar isotopic compositions of stem, shallow soil, and stream water suggest that mixing and damping of fog signature has occurred, possibly due to small fog volumes and a larger soil moisture reservoir. Furthermore, the isotopic results confirm that soil water pools are simultaneously contributing to vegetation uptake and streamflow, whereas the difference in signature between fog and streamflow suggests an absence of direct fog water isotopic input in the watershed's surface waters. These results relate to the challenges in fog water tracing through isotope signatures, as streamflow isotopes are temporally invariant and mixing can average out the signal of individual fog events (Brooks, Barnard, Coulombe, & McDonnell, 2010; Kennedy, Kendall, Zellweger, Wyerman, & Avanzino, 1986; Oshun, Dietrich, Dawson, & Fung, 2016).

Avoided transpiration, from reduced vapour pressure deficits during fog events resulting in decreased transpiration demand from vegetation, however, is more significant, along the lines of 125 mm/year. Decreased fog interception and deposition in chaparral likely results in a smaller change in transpiration demand when compared to Douglas fir trees, whose canopy is able to capture more moisture from fog due to canopy height and shape. The high PET rates under forest canopy on clear days, which can comprise nearly half of the dry season, signal a potential offset of water savings accrued during preceding fog events. Yet we must note that these additional inputs and reduced losses occur during the dry season, alleviating the watershed water deficit during this time from 570 to 430 mm, a 25% decrease. This is comparable to previous findings that show that fog can comprise 13–45% of annual transpiration in a heavily fog-inundated coastal forest (Dawson, 1998). These contributions to the dry-season water balance can relieve the watershed's low flow conditions that serve as a major stressor for anthropogenic and natural processes and are thus non-trivial.

Estimation and evaluation of such watershed-scale effects of fog are dependent on the upscaling scheme, and specifically, the data sources and interpolation methods used. Commonly-used spatial interpolations to estimate a watershed-averaged flux, including Thiessen polygons and inverse distance weighting, are limited by heavy dependence on the location and density of sampling points, whereas kriging methods cannot incorporate the wide array of watershed features that may be spatially correlated to throughfall, producing inaccurate isohyetal fog patterns. The presented scheme, however, reflects the spatial patterns of a watershed's fog events observed by remote sensing and incorporates a suite of sensors that is able to capture the spatial range of vegetation cover and topography to predict the watershed-scale fog water flux (Figure 11).

In our upscaling scheme, both watershed vegetation and elevation influence fog water flux, consistent with models of deposition over heterogeneous terrain (Weathers, Simkin, Lovett, & Lindberg, 2006). Vegetation effects, however, are more pronounced than the topographic effects, with greater sensitivity of fog water flux estimates to vegetation than elevation information. As observed by Weathers et al. (2006), though high elevation sites have large potential for high throughfall volumes due to frequent fog occurrence, this potential is captured and high volumes are observed where coniferous forest canopy, with large leaf surface area, occurs at high elevations. Therefore, the throughfall collectors and watershed vegetation map, which characterize the difference in throughfall under heterogeneous canopies in the basin, have higher information value than the leaf wetness sensors and DEM, which quantify the varying moisture conditions along a topographic gradient. We note that we have assumed collinearity between distance from forest edge and elevation in the Upper Pilarcitos Creek watershed, and this may result in an over-estimation of watershed-scale flux by not including possible non-linear forest edge effects along an elevation band. Reducing the number of throughfall collectors in the scheme decreases the watershed area for which there is information, forcing two assumptions: (a) larger portions of the watershed are experiencing zero effects from fog or (b) the spatial effects of fog are more uniform than in reality. This first assumption results in an underestimate of watershed-scale estimates, whereas the second assumption can also produce an underestimate if the included throughfall collectors are placed in an area that experiences minimal fog effects. On the other hand, reducing the number of leaf wetness sensors in this placement, along a topographic gradient, does not affect the inference of spatial coverage of the watershed under the influence fog. It does worsen; however, the accuracy of the elevation gradient by obscuring identification of elevation-dependent spatial patterns of fog events and deposition. Lastly, failing to condition the interpolation polygons on observed spatial patterns of fog (i.e., by including Landsat data) leads to higher estimates because often, areas that are rarely fog-covered, and thus a larger percentage of the watershed, are assumed to experience fog.

When estimating a watershed-scale fog water flux, sensor instrumentation governs appropriate spatial interpolation. The watershed's dominant vegetation types should first be identified, and differences in fog interception and deposition under the different vegetation canopies should be closely monitored and compared through installation of multiple throughfall collectors. The throughfall collectors should be deployed strategically to span the non-random spatial patterns of fog, which can be inferred from remote sensing imagery prior to field work and data collection. Assuming that the location and density of throughfall collectors cover the full spatial extent of fog events, deployment of leaf wetness sensors along a topographic gradient can be useful in understanding elevation effects. Leaf wetness sensors
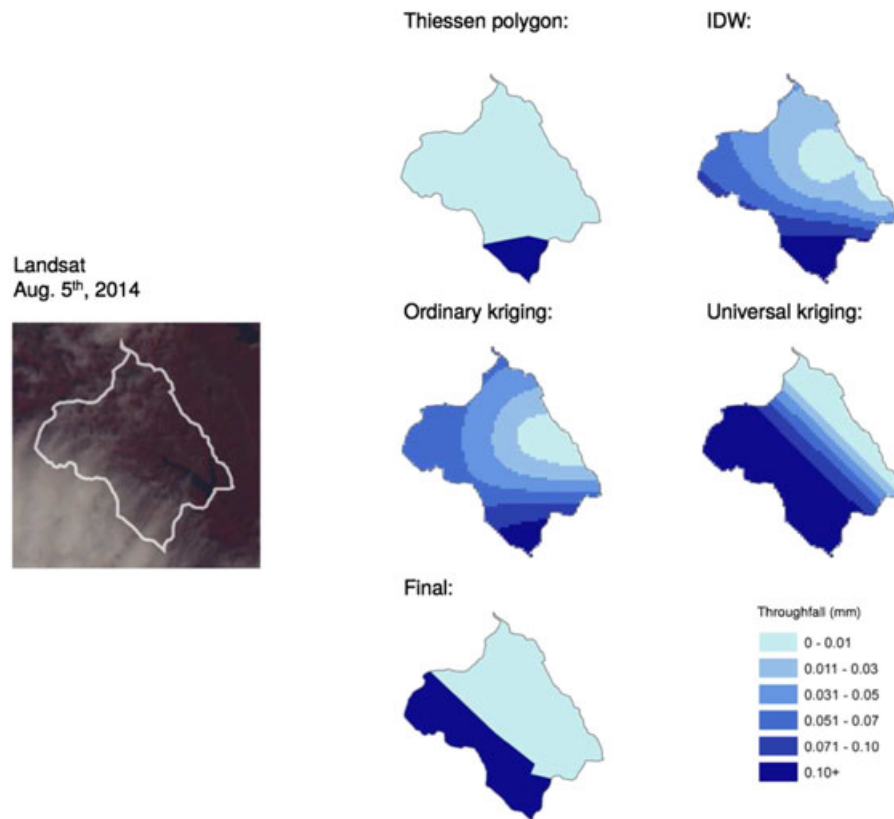
FIGURE 11 The final upscaling scheme captures spatial heterogeneities and reflects actual fog patterns observed in the watershed via Landsat 8 (cf. standard spatial interpolation methods)

could be installed along a topographic gradient to further elucidate the spatial patterns of fog; at least three leaf wetness sensors should be deployed along the gradient, as the elevation effects on throughfall may be non-linear in some cases. Additional monitoring across different topographic gradients are desirable, but may be practically limited by access and safety considerations. Furthermore, in this study, there was only one site where leaf wetness sensors and throughfall collectors were co-located. Due to throughfall's high spatial variability, more extensive calibration of throughfall–leaf wetness relationships across multiple sites, canopy conditions, and vegetation types could allow a wider use of relatively inexpensive leaf wetness sensors as a proxy for fog-derived moisture. In coastal watersheds similar to the Upper Pilarcitos Creek Watershed, where elevation and vegetation are independent, both vegetation and elevation data are required for upscaling. Deployment of sensors in multiple co-located sites can capture variability under similar fog exposure and canopy and reduce the uncertainty in regression for improved scaling of throughfall. In watersheds where vegetation and elevation are correlated, both sets of data may not be required. The polygons within the interpolation scheme should be created from a combination of remotely-sensed fog patterns and distance-based methods to accurately identify and delineate watershed areas that experience fog. For larger-scale applications, we suggest employing automated image processing of time-lapse imagery for fog detection due to the labour-intensive nature of data processing. This combination of sensors, time-lapse imagery, and remote sensing allows observation of heterogeneities in fog events and deposition to be upscaled to a spatially-averaged flux to evaluate fog's effects on the watershed hydrologic balance.

5 | CONCLUSION

Watersheds with frequent occurrence of fog events experience water stress relief during the dry summer months, but fog's quantitative effects on the water balance of a basin are less well known. To better understand fog's hydrologic role during the dry season, the dominant controls on spatial and temporal heterogeneity of fog events must be identified. This study presents a novel stratified sampling plan using a suite of sensors, time-lapse imagery, and remote sensing data, as well as an upscaling scheme that combines these datasets to estimate watershed-scale fog water fluxes and evapotranspiration suppression. The upscaling scheme allows evaluation of the mechanisms through which fog contributes to the overall water budget: We find that although fog interacts with the water balance directly via a fog water flux and climatically through reduced evapotranspiration suppression in the Upper Pilarcitos Creek Watershed, the avoided transpiration provides a more significant relief of summer watershed water deficit. Fog is therefore critical in regions such as northern coastal California, where precipitation and transpiration are out of phase and high terrestrial and aquatic ecosystem demand for water coincides with the dry season.

ORCID

Michaella Chung http://orcid.org/0000-0002-6651-9441

REFERENCES

Azevedo, J., & Morgan, D. (1974). Fog precipitation in coastal California forests. *Ecology*, *55*, 1135–1141.

Bacchi, Baldassare, & Kottegoda, N. T. (1995). Identification and calibration of spatial correlation patterns of rainfall. *Journal of Hydrology, 165*, 311–348.

Breazeale, E., McGeorge, W., & Breazeale, J. (1950). Moisture absorption by plants from an atmosphere of high humidity. *Plant Physiology, 25*, 413–419.

Brooks, J. R., Barnard, H. R., Coulombe, R., & McDonnell, J. J. (2010). Ecohydrologic separation of water between trees and streams in a Mediterranean climate. *Nature Geoscience, 3*, 100–104.

Burgess, S., & Dawson, T. (2004). The contribution of fog to the water relations of Sequoia sempervirens (D. Don): Foliar uptake and prevention of dehydration. *Plant, Cell and Environment, 27*, 1023–1034.

Dale, M. R., & Fortin, M. J. (2014). *Spatial analysis: A guide for ecologists.* Cambridge, UK: Cambridge University Press.

Dawson, T. E. (1996). The use of fog precipitation by plants in coastal redwood forests. In *Conference on Coastal Redwood Forest Ecology and Management, Humboldt State University*, pp. 90–93. Arcata, CA, USA.

Dawson, T. (1998). Fog in the California redwood forest: Ecosystem inputs and use by plants. *Oecologia, 117*, 476–485.

Ewing, H., Weathers, K., Templer, P., Dawson, T., Firestone, M., Elliott, A., & Boukili, V. (2009). Fog water and ecosystem function: Heterogeneity in a California redwood forest. *Ecosystems, 12*, 417–433.

Fischer, D. T., & Still, C. J. (2007). Evaluating patterns of fog water deposition and isotopic composition on the California Channel Islands. *Water Resources Research, 43*, 1–13.

Fischer, D., Still, C., & Williams, A. (2009). Significance of summer fog and overcast for drought stress and ecological functioning of coastal California endemic plant species. *Journal of Biogeography, 36*, 783–799.

Garreaud, R., Barichivich, J., Christie, D. A., & Maldonado, Antonio (2008). Interannual variability of the coastal fog at Fray Jorge relict forests in semiarid Chile. *Journal of Geophysical Research: Biogeosciences, 113*, 1–16.

Haines, F. (1952). The absorption of water by leaves in an atmosphere of high humidity. *Journal of Experimental Botany, 3*, 95–98.

Haines, F. (1953). The absorption of water by leaves in fogged air. *Journal of Experimental Botany, 4*, 106–107.

Harr, R. (1980). Streamflow after patch logging in small drainages within the Bull Run Municipal watershed, Oregon. USDA Forest Service Research Paper, PNW-268.

Harr, R. (1982). Fog drip in the Bull Run Municipal Watershed, Oregon. *Water Resources Bulletin, 18*, 785–789.

Hiatt, C., Fernandez, D., & Potter, C. (2012). Measurements of fog water deposition on the California Central Coast. *Atmospheric and Climate Sciences, 2*, 525–531.

Hutley, L., Doley, D., Yates, D., & Boonsaner, A. (1997). Water balance of an Australian subtropical rainforest at altitude: The ecological and physiological significance of intercepted cloud and fog. *Australian Journal of Botany, 45*, 311–329.

Ingraham, N., & Matthews, R. (1988). Fog drip as a source of groundwater recharge in northern Kenya. *Water Resources Research, 24*, 1406–1410.

Ingraham, N., & Matthews, R. (1995). The importance of fog-drip water to vegetation: Point Reyes Peninsula, California. *Journal of Hydrology, 164*, 269–285.

Ingwersen, J. (1985). Fog drip, water yield, and timber harvesting in the Bull Run Municipal Watershed, Oregon. *Water Resources Bulletin, 21*, 469–473.

Johnstone, J., & Dawson, T. (2010). Climatic context and ecological implications of summer fog decline in the coast redwood region. *Proceedings of the National Academy of Sciences, 107*, 4533–4538.

Juvik, J. O., & Nullet, Dennis (1995). Comments on "A proposed standard fog collector for use in high-elevation regions". *Journal of Applied Meteorology, 34*(9), 2108–2110.

Kennedy, V., Kendall, C., Zellweger, G., Wyerman, T., & Avanzino, R. (1986). Determination of the components of stormflow using water chemistry and environmental isotopes, Mattole River basin, California. *Journal of Hydrology, 84*, 107–140.

Keppeler, E. (2007). Effects of timber harvest on fog drip and streamflow, Caspar Creek Experimental Watersheds, Mendocino County, California. In *Redwood Science Symposium: What does the future hold?* pp. 85–93. Albany, CA, USA.

Koohafkan, M., Thompson, S. E., & Dawson, T. E. (2014, unpublished material). Can dielectric leaf wetness sensors be used to quantify surface water storage on leaves of Californian tree species?

Leipper, D. (1995). Fog forecasting objectively in the California coastal area using LIBS. *Weather Forecast, 10*, 741–762.

Mooney, H., & Zavaleta, E. (2016). *Ecosystems of California.* Oakland, CA, USA: Univ of California Press.

NOAA Office of Satellite and Product Operations (2015). Operational SST Anomaly Charts for 2016. http://www.ospo.noaa.gov/Products/ocean/sst/anomaly.

Oberlander, G. (1956). Summer fog precipitation on the San Francisco peninsula. *Ecology, 37*, 851–852.

Oshun, Jasper, Dietrich, W. E., Dawson, T. E., & Fung, Inez (2016). Dynamic, structured heterogeneity of water isotopes inside hillslopes. *Water Resources Research, 52*, 164–189.

Peace, R. J. (1969). Heavy-fog regions in the conterminous United States. *Monthly Weather Review, 97*, 116–123.

Potter, C. (2016). Measurements of fog water interception by shrubs on the California central coast. *Journal of Coastal Conservation, 20*, 315–325.

Prada, S., & da Silva, M. (2001). Fog precipitation on the Island of Madeira (Portugal). *Environmental Geology, 41*, 384–389.

Priestley, C., & Taylor, R. (1972). On the assessment of surface heat flux and evaporation using large scale parameters. *Monthly Weather Review, 100*, 81–92.

Sawaske, S., & Freyberg, D. (2015). Fog, fog drip, and streamflow in the Santa Cruz Mountains of the California Coast Range. *Ecohydrology, 8*, 695–713.

Schemenauer, R., & Cereceda, P. (1991). Fog-water collection in arid coastal locations. *Ambio, 20*, 303–308.

Scholl, M., Gingerich, S., & Tribble, G. (2002). The influence of microclimates and fog on stable isotope signatures used in interpretation of regional hydrology: East Maui, Hawaii. *Journal of Hydrology, 264*, 170–184.

Shuttleworth, W. (1977). The exchange of wind-driven fog and mist between vegetation and the atmosphere. *Boundary-Layer Meteorology, 12*, 463–489.

Templer, P. H., Weathers, K. C., Ewing, H. A., Dawson, T. E., Mambelli, S., Lindsey, A. M., … Firestone, M. K. (2015). Fog as a source of nitrogen for redwood trees: Evidence from fluxes and stable isotopes. *Journal of Ecology, 103*(6), 1397–1407.

Vogl, R. (1973). Ecology of knobcone pine in the Santa Ana Mountains, California. *Ecological Monographs, 43*, 125–143.

Wang, L., Kaseke, K. F., & Seely, M. K. (2017). Effects of non-rainfall water inputs on ecosystem functions. *Wiley Interdisciplin Review: Water, 4*(1), 1–18.

Wang, W., Anderson, B., Phillips, N., Kaufmann, R., Potter, C., & Myneni, R. (2006). Feedbacks of vegetation on summertime climate variability over the North American Grasslands. Part I: Statistical analysis. *Earth Interactions, 10*, 1–27.

Weathers, K. C., Simkin, S. M., Lovett, G. M., & Lindberg, S. E. (2006). Empirical modeling of atmospheric deposition in mountainous landscapes. *Ecological Applications, 16*(4), 1590–1607.

Weathers, K., Lovett, G., & Likens, G. (1995). Cloud deposition to a spruce forest edge. *Atmospheric Environment, 29*, 665–672.

Weathers, K., Lovett, G., Likens, G., & Caraco, N. (2000). Cloudwater inputs of nitrogen to forest ecosystems in southern Chile: Forms, fluxes, and sources. *Ecosyst, 3*, 590–595.